Therapeutics, Targets, and Chemical Biology

Cancer Research

eIF4E/4E-BP Ratio Predicts the Efficacy of mTOR Targeted Therapies

Tommy Alain[1,5], Masahiro Morita[1,5], Bruno D. Fonseca[1,5], Akiko Yanagiya[1,5], Nadeem Siddiqui[1,5], Mamatha Bhat[1,5,6], Domenick Zammit[1,5,7], Victoria Marcus[7], Peter Metrakos[2,8,9], Lucie-Anne Voyer[1,5], Valentina Gandin[4], Yi Liu[10], Ivan Topisirovic[3,4], and Nahum Sonenberg[1,3,5]

Abstract

Active-site mTOR inhibitors (asTORi) hold great promise for targeting dysregulated mTOR signaling in cancer. Because of the multifaceted nature of mTORC1 signaling, identification of reliable biomarkers for the sensitivity of tumors to asTORi is imperative for their clinical implementation. Here, we show that cancer cells acquire resistance to asTORi by downregulating eukaryotic translation initiation factor (eIF4E)-binding proteins (4E-BPs—*EIF4EBP1*, *EIF4EBP2*). Loss of 4E-BPs or overexpression of eIF4E renders neoplastic growth and translation of tumor-promoting mRNAs refractory to mTOR inhibition. Conversely, moderate depletion of eIF4E augments the anti-neoplastic effects of asTORi. The anti-proliferative effect of asTORi *in vitro* and *in vivo* is therefore significantly influenced by perturbations in eIF4E/4E-BP stoichiometry, whereby an increase in the eIF4E/4E-BP ratio dramatically limits the sensitivity of cancer cells to asTORi. We propose that the eIF4E/4E-BP ratio, rather than their individual protein levels or solely their phosphorylation status, should be considered as a paramount predictive marker for forecasting the clinical therapeutic response to mTOR inhibitors. *Cancer Res; 72(24); 6468–76. ©2012 AACR.*

Introduction

mTOR is a multifunctional serine/threonine kinase, which exists in 2 distinct complexes, mTOR complex 1 and 2 (mTORC1 and 2; ref. 1). mTORC1 governs many cellular processes including mRNA translation, cell growth, and proliferation, by phosphorylating downstream targets such as 4E-BPs and S6Ks (1). mTORC2 controls cell survival and cytoskeleton organization by modulating the activity of AGC kinases (e.g., Akt and SGK1) and regulates nascent polypeptide stability (2). Hyperactivation of mTOR signaling frequently occurs in cancer (in more than 70% of patients; ref. 3). Therefore, targeting mTOR represents one of the most attractive anti-cancer therapeutic strategies. Rapamycin, a naturally occurring allosteric inhibitor of mTORC1, and its analogues (rapalogs), are clinically approved for treatment of renal cell carcinomas, mantle cell lymphomas, and pancreatic neuroendocrine tumors (4, 5). Nonetheless, the overall success of rapalog monotherapies is limited. This has been attributed to the incomplete inhibition of mTORC1-mediated phosphorylation of 4E-BPs, and the activation of Akt via the loss of a negative feedback mechanism (4, 6, 7). Recently, asTORi (also referred to as TORKin or dual mTORC1/mTORC2 inhibitors) were developed to overcome these issues. asTORi abolish phosphorylation of 4E-BPs via the inhibition of mTORC1, suppress Akt signaling via the inhibition of mTORC2, and exhibit stronger anti-proliferative and anti-tumorigenic effects than rapamycin (8–11). However, mTOR regulates various cancer-related processes via a multitude of substrates, and this complexity of mTOR signaling represents a significant challenge for identifying surrogate biomarkers that could serve to predict the efficacy of asTORi in the clinic (12).

eIF4E is the 5′ mRNA cap-binding subunit of the eIF4F complex, which recruits mRNA to the ribosome. eIF4F also includes the large scaffolding protein eIF4G and the DEAD-box RNA helicase eIF4A (13, 14). 4E-BPs (in mammals 4E-BP1, 2, and 3) are small-molecular-weight translational repressors, which impair the assembly of the eIF4F complex by competing with eIF4G for binding to eIF4E (14, 15). mTORC1 phosphorylates 4E-BPs leading to their dissociation from eIF4E, thus increasing the amount of eIF4E available to engage in the eIF4F complex assembly (15–17). Ectopic expression of eIF4E leads

Authors' Affiliations: Departments of [1]Biochemistry, [2]Anatomy and Cell Biology, and [3]Oncology, [4]Lady Davis Institute for Medical Research, SMBD-Jewish General Hospital, [5]Goodman Cancer Research Centre, [6]Division of Gastroenterology, Department of Medicine, Departments of [7]Pathology and [8]Surgery, Hepatopancreatobiliary and Transplant Research Unit, McGill University Health Centre, Montreal, Quebec, Canada; [9]Department of Surgery, College of Medicine, King Saudi University, Riyadh, Saudi Arabia; and [10]Intellikine, La Jolla, California

Note: Supplementary data for this article are available at Cancer Research Online (http://cancerres.aacrjournals.org/).

T. Alain and M. Morita contributed equally to this work.

Corresponding Authors: Nahum Sonenberg, James McGill Professor, McGill University, Department of Biochemistry, Goodman Cancer Research Centre, 1160, Avenue Des Pins Ouest, Cancer Pavilion, Room #615, Montréal, Québec, H3A 1A3, Canada. Phone: 514-398-7274; Fax: 514-398-1287; E-mail: nahum.sonenberg@mcgill.ca; and Ivan Topisirovic, Lady Davis Institute for Medical Research, Department Of Oncology, McGill University, Sir Mortimer B. Davis Jewish General Hospital, Office E-445, 3755 Côte Ste-Catherine Road, Montreal, Quebec H3T 1E2, Canada. Phone: 514-340-8222, ext. 3146; E-mail: ivan.topisirovic@mcgill.ca

doi: 10.1158/0008-5472.CAN-12-2395

to transformation of immortalized rodent and human cells (18, 19) and is tumorigenic *in vivo* (20). About 30% of cancers exhibit elevated eIF4E levels, which correlate with poor prognosis (21). eIF4E overexpression induces cell transformation by selectively augmenting translation of mRNAs referred to as eIF4E-sensitive mRNAs, which encode proliferation- and survival-promoting proteins (e.g., cyclins, c-myc, and Bcl-xL; refs. 18, 22). Multiple factors can induce the overexpression of eIF4E in cancer cells including gene amplification (23), transcriptional upregulation by c-myc (24), and increase in eIF4E mRNA stability by HuR (25). Dysregulated expression and/or increased phosphorylation of 4E-BPs in cancer have also been linked to poor patient outcomes (21, 26). 4E-BPs mediate the effects of mTOR signaling on translation of mRNAs that encode proteins that are associated with cancer progression, invasion, and metastasis (e.g., Y-box protein 1, vimentin, and CD44; ref. 11). 4E-BP1 expression is controlled at the transcriptional and protein stability levels by ATF4 (27) and the KLHL25-CUL3 complex (28), respectively.

In this study, we show that cancer cells acquire resistance to asTORi by increasing eIF4E availability via downregulation of 4E-BP1 and 2. Accordingly, we show that an increase in eIF4E, or reduction in 4E-BP levels by RNA interference, strongly attenuates the anti-neoplastic effects of the asTORi PP242, Torin1, and INK1341 (an analogue of the recently characterized INK128 compound; ref. 11). Conversely, a decrease in the eIF4E/4E-BP ratio ameliorates the inhibitory effects of asTORi on translation of eIF4E-sensitive cyclin D3 and E1 mRNAs. Thus, the eIF4E/4E-BP ratio in the tumor could be a significant predictive marker of the efficacy of asTORi that should be considered in devising personalized asTORi treatments.

Materials and Methods

Cell culture, constructs, viral infections, and lentiviral shRNA silencing

E1A/Ras-transformed WT ($p53^{-/-}$) and 4E-BP1/2 DKO ($p53^{-/-}$) mouse embryonic fibroblasts (MEF), referred to as $WT^{E1A/Ras}$ and 4E-BP1/2 $DKO^{E1A/Ras}$ MEFs respectively, were previously described (7). HeLa, SK-HEP-1, and HepG2 cells were directly purchased from and authenticated by American Type Culture Collection. Cells were maintained in Dulbecco's Modified Eagle's Medium (DMEM; Invitrogen), supplemented with 10% FBS (Invitrogen), 2 mmol/L L-glutamine, and 100 units/mL penicillin/streptomycin (all from Invitrogen) at 37°C and 5% CO_2. To induce acquired resistance to asTORi, $WT^{E1A/Ras}$, HepG2 and SK-HEP-1 cell lines were cultured in the continuous presence of the PP242 (1 μmol/L for 8 weeks). NIH3T3 cells transduced with pMV7-eIF4E or empty vector (pMV7) were described previously (18). For overexpression studies, pcDNA3-3HA-4E-BP1 (4E-$BP1^{WT}$) and pACTAG2-3HA-4E-BP1 (4E-$BP1^{\Delta 4E}$) have been described previously (29, 30). 4E-BP1 and mutant cDNA were amplified by PCR and inserted into *Bam*HI/*Sal*I sites of the retroviral vector pBABE. Cell lines that stably express 4E-BP1 were generated as described previously (31). Briefly, pBABE constructs were transiently transfected into the Ecotropic Phoenix-293T packaging cell line. After 48 hours, virus-containing medium was filtered (0.45 μm), collected, and used to infect MEFs in the presence of 5 μg/mL polybrene (Sigma-Aldrich). Infection was repeated the next day. Twenty-four hours after the second infection, medium supplemented with puromycin (1 μg/mL, Sigma-Aldrich) was added, and cells were subjected to selection for 1 week, after which time colonies were pooled. pcDNA3-FLAG-eIF4E^{WT} and eIF4E^{W56A} (cap-binding mutant) were constructed by cloning the entire coding sequence of mouse eIF4E into pcDNA3-FLAG using a PCR (32). These vectors were transfected and cells selected in G418 for 2 weeks. Lentiviral vectors were from Sigma. Short hairpin RNA (shRNA) vector accession numbers are: mouse eIF4E (Sigma: TRCN0000077474), the Non-Target shRNA Control (Sigma: SHC002). shRNA vectors were co-transfected into HEK293T cells with the lentivirus packaging plasmids PLP1, PLP2, and PLP-VSVG (Invitrogen) using Lipofectamine 2000 (Invitrogen). Supernatants were collected 48 and 72 hours posttransfection, passed through a 0.45-μm nitrocellulose filter, and applied on target cells with polybrene (5 μg/mL). Cells were re-infected the next day and selected with puromycin for 48 hours (1 μg/mL, Sigma). PP242 and INK1341 were provided by Intellikine. Torin1 was from N. Gray and D. Sabatini.

Cell-cycle analysis and apoptosis

Cells were seeded in 100-mm dishes, grown overnight, and treated as indicated in figure legends. Twenty-four or 48 hours later, cells were harvested by trypsinization, washed twice with PBS containing 2% FBS and once in PBS. For cell-cycle analysis, cells were resuspended in 200 μL of NPE Nuclear Isolation Media (NIM)-DAPI (Beckman Coulter) and analyzed using a Cell Lab Quanta SC (Beckman Coulter) flow cytometer. For apoptosis, cells were analyzed by flow cytometry using the Annexin V-FITC Apoptosis Detection Kit according to the manufacturer's protocol (Bio Vision).

Cell proliferation, soft agar, and anchorage-dependent foci formation assay

For the bromodeoxyuridine (BrdU) incorporation assay (Cell Proliferation ELISA BrdU Kit from Roche), cells were seeded in 96-well plates (1,000 cells/well) and maintained as indicated in the figure legends. Absorbance at 370 nm (reference wavelength = 492 nm) was measured using a Varioskan microplate reader (Thermo Electron Corporation). For Trypan blue exclusion, cells were seeded in 6-well plates (50,000 cells/well) overnight and maintained under conditions outlined in the figure legends. Cell proliferation was determined by direct counting (dead cells were excluded by Trypan blue staining). For soft agar assays, experiments were carried out in 6-well plates coated with a base layer of 0.5% agarose (Agar Noble, Difco). $WT^{E1A/Ras}$ and 4E-BP1/2 $DKO^{E1A/Ras}$ MEFs were seeded in triplicates at a density of 5,000 cells/well in 0.35% agarose containing either vehicle [dimethyl sulfoxide (DMSO)], PP242 (1 μmol/L), or INK1341 (250 nmol/L). Cells were overlaid with DMEM supplemented with 10% FBS, 2 mmol/L L-glutamine, and 100 units/mL penicillin/streptomycin (Invitrogen) containing either DMSO, PP242 (1 μmol/L), or INK1341 (nmol/L), and incubated for up to 10 to 14 days. Media containing vehicle, PP242, or INK1341 were changed every 3 to 4 days during the course of the experiment. Colonies were counted using a light

microscope. For focus formation assays, cells were seeded at a density of 10,000 cells/10-cm dish and allowed to grow in the presence of either vehicle (DMSO) or PP242 (1 μmol/L) or INK1341 (250 nmol/L). Media containing drugs were changed as above every 3 to 4 days.

Western blot analysis and cap (m^7GDP) pull-down assay

Cell lysates were prepared, and Western blotting was carried out as described (33). Antibodies against 4E-BP1, 4E-BP2, phospho-4E-BP1 (Thr37/46, Ser65, Thr70), rpS6, phospho-rpS6 (Ser240/244), Akt, phospho-Akt (S473), eIF4G1, and cyclin D3 were from Cell Signaling Technology (Danvers, MA). Antibody against cyclin E1 was from Santa Cruz Biotechnology. Antibodies against eIF4E and β-actin were from Sigma. Horseradish peroxidase (HRP)-conjugated anti-rabbit IgG and anti-mouse IgG were from Amersham Biosciences. For cap-binding affinity assay, cells were lysed in the lysis buffer [50 mmol/L HEPES-KOH (pH 7.5), 150 mmol/L KCL, 1 mmol/L EDTA, 2 mmol/L dithiothreitol (DTT), and 0.2% Tween] containing protease inhibitors. Cell lysates were incubated with m^7GDP-agarose and washed 4 times using the lysis buffer. m^7GDP-bound proteins were determined by Western blotting.

Polysome analysis, RNA isolation, and sqRT-PCR

Polysome profile analysis was carried out as previously described (34). Briefly, cells were cultured in 15-cm dishes and treated with PP242 (1 μmol/L), INK1341 (250 nmol/L), or vehicle (DMSO) for 8 hours. Cells were washed with cold PBS containing 100 μg/mL cycloheximide, collected, and lysed in a hypotonic lysis buffer [5 mmol/L Tris-HCl (pH 7.5), 2.5 mmol/L $MgCl_2$, 1.5 mmol/L KCl, 100 μg/mL cycloheximide, 2 mmol/L DTT, 0.5% Triton X-100, and 0.5% sodium deoxycholate). Lysates were loaded onto 10% to 50% sucrose density gradients [20 mmol/L HEPES-KOH (pH 7.6), 100 mmol/L KCl, 5 mmol/L $MgCl_2$] and centrifuged at 36,000 rpm for 2 hours at 4°C. Gradients were fractionated, and the optical density (OD) at 254 nm was continuously recorded using an ISCO fractionator (Teledyne ISCO). RNA from each fraction was isolated using TRIzol (Invitrogen) and treated with DNaseTurbo (Ambion) according to the manufacturer's instructions. Reverse transcription PCR (RT-PCR) and quantitative RT-PCR (qRT-PCR) reactions were carried out using SuperScript III First-Strand Synthesis System (Invitrogen) and iQ SYBR Green Supermix (BIO-RAD) according to the manufacturer's instructions. The list of primers and the number of cycles used for each of the transcripts were described (7).

Tumor growth curves

Six- to 8-week-old $Nude^{NCR}$ (*nu*/*nu*) mice were obtained from Taconic. The animals were maintained under specific pathogen-free conditions and treated according to a protocol approved by the McGill University Animal Care Committee (Montreal, QC, Canada). A total of 5×10^6 $WT^{E1A/Ras}$ and 4E-BP1/2 $DKO^{E1A/Ras}$ MEFs in 100 μL PBS were injected in the hind flank of the mice and allowed to grow until palpable tumors were established. For drug treatment, PP242 at 60 mg/kg in a solution containing 40% PEG-400, 40% PBS, and 20% DMSO was administrated intraperitoneally in 100 μL volume. Two-dimensional tumor measurements were conducted with calipers every other day for 10 days or until the animals showed severe complications due to excess tumor burden.

Statistical analysis

Error bars for all data represent SDs from the mean. *P* values were calculated using Student *t* tests.

Results

Acquired resistance to asTORi coincides with downregulation of 4E-BP1 and 2 expression

To investigate the potential mechanism of acquired resistance to asTORi in cancer cells, we cultivated E1A/Ras-transformed $p53^{-/-}$ MEFs ($WT^{E1A/Ras}$) and 2 liver cancer cell lines (HepG2 and SK-HEP-1) in the presence of the asTORi PP242 (1 μmol/L for 8 weeks). Strikingly, all 3 cell lines acquired resistance to PP242, which correlated with a downregulation of 4E-BP1 and 2 (Figs. 1A–C; Supplementary Fig. S1A–S1F), but not with a loss of mTORC1 or 2 inhibition, inasmuch as asTORi induced similar suppression of ribosomal protein S6 (S6) and Akt phosphorylation in resistant and control cells (Supplementary Fig. S1G and S1H).

To ascertain that 4E-BPs are responsible for the anti-neoplastic activity of asTORi, we investigated the effects of PP242 on the neoplastic growth of $WT^{E1A/Ras}$ and E1A/Ras-transformed $p53^{-/-}/4e\text{-}bp1/2^{-/-}$ MEFs (4E-BP $DKO^{E1A/Ras}$). 4E-BP $DKO^{E1A/Ras}$ MEFs are devoid of all 4E-BPs, as MEFs do not express 4E-BP3 (7). $WT^{E1A/Ras}$ and 4E-BP $DKO^{E1A/Ras}$ MEFs proliferated at the same rate in full growth medium (Fig. 1D) where mTOR activity is high and 4E-BP1 and S6 are hyperphosphorylated (Fig. 1E). However, while PP242 inhibits mTORC1 signaling to a similar extent in these cells, as illustrated by a comparable reduction in the phosphorylation of S6 (Fig. 1E), the effects of PP242 on neoplastic growth were significantly less pronounced in 4E-BP $DKO^{E1A/Ras}$ MEFs (∼45% reduction in number of colonies and foci relative to control) than in $WT^{E1A/Ras}$ MEFs (∼70%; Figs. 1F and G; Supplementary Fig. S2A–S2C). Moreover, depletion of 4E-BP1 and 2 rendered neoplastic growth of SK-HEP-1 and HepG2 cells partially resistant to PP242 (Supplementary Figs. S1A–S1C and S2D–S2F). These results show that loss of 4E-BPs attenuates the anti-neoplastic efficacy of asTORi.

Increased eIF4E availability renders cells resistant to asTORi

When mTOR signaling is inhibited, 4E-BPs limit the fraction of eIF4E available for the assembly of the eIF4F complex (15–17). Thus, we investigated whether the sequestration of eIF4E by 4E-BPs is required for the anti-neoplastic activity of INK1341 by overexpressing $4E\text{-}BP1^{WT}$ and $4E\text{-}BP1^{\Delta 4E}$ mutant, which lacks the eIF4E-binding motif and thus cannot bind eIF4E (ref. 35; Fig. 1H). Expression of $4E\text{-}BP1^{WT}$, but not $4E\text{-}BP1^{\Delta 4E}$, augmented the anti-neoplastic effect of INK1341 (Figs. 1I and J). Moreover, forced expression of $4E\text{-}BP1^{WT}$ markedly reduced the association between eIF4E and eIF4G1 as compared with a control (Supplementary Fig. S2G and S2H). Taken together, these results show that 4E-BPs mediate the anti-tumorigenic activity of asTORi by limiting the availability of eIF4E to associate with eIF4G1, thereby impeding the eIF4F complex assembly.

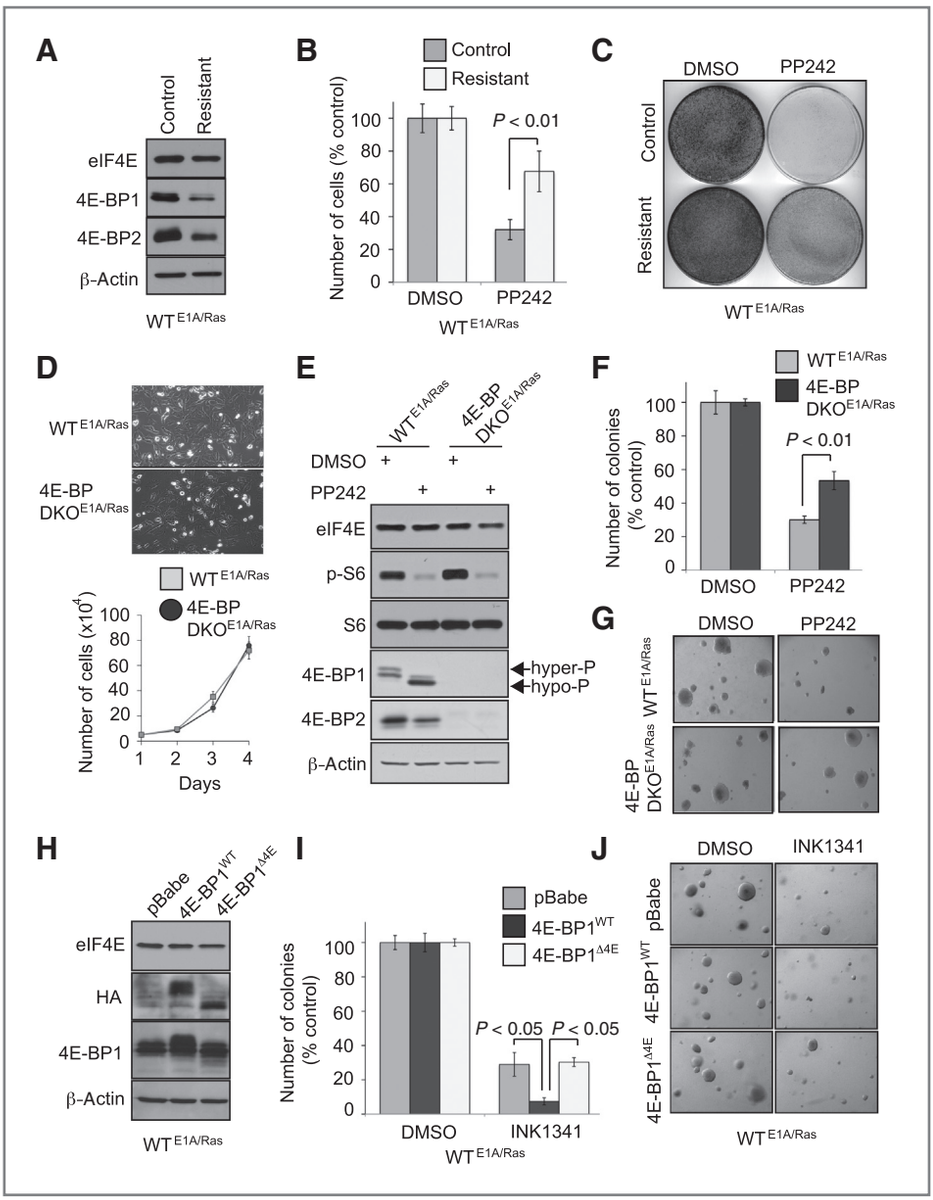

Figure 1. 4E-BP1 and 2 downregulation underlies acquired resistance to asTORi. A, Western blot analysis of the indicated proteins in $WT^{E1A/Ras}$ MEFs maintained in the presence of DMSO (control) or PP242 (1 μmol/L) for a period of 8 weeks. β-Actin served as a loading control. B, resistant and control $WT^{E1A/Ras}$ MEFs were treated with PP242 (1 μmol/L) for 7 days, and cell proliferation was determined by Trypan blue exclusion. Results represent the mean cell number relative to a DMSO control (set to 100%) ± SD ($n = 3$). C, cells described in B were stained with crystal violet. D, phase contrast images of $WT^{E1A/Ras}$ or 4E-BP $DKO^{E1A/Ras}$ MEFs (top). Proliferation rates of $WT^{E1A/Ras}$ or 4E-BP $DKO^{E1A/Ras}$ MEFs in full growth medium were determined by Trypan blue exclusion (bottom). Results are presented as mean numbers of cells ± SD ($n = 3$). E, $WT^{E1A/Ras}$ or 4E-BP $DKO^{E1A/Ras}$ MEFs were treated with DMSO or PP242 (1 μmol/L) for 3 hours. Levels and the phosphorylation status of the indicated proteins were determined by Western blot analysis. β-Actin served as a loading control. Arrows indicate the hyperphosphorylated (hyper-P) and hypophosphorylated (hypo-P) forms of 4E-BP1. F, effects of DMSO and PP242 (1 μmol/L) on anchorage-independent growth of $WT^{E1A/Ras}$ and 4E-BP $DKO^{E1A/Ras}$ MEFs were monitored using a soft agar assay. Colonies were counted after 10 days of treatment. Results are presented as a mean number of colonies relative to a DMSO control (set to 100%) ± SD ($n = 3$). G, representative photographs of colonies formed by the cells described in F. H, $WT^{E1A/Ras}$ MEFs were transduced with an empty vector (pBABE) or vector expressing hemagglutinin (HA)-tagged wild-type 4E-BP1 ($4E\text{-}BP1^{WT}$) or $4E\text{-}BP1^{\Delta 4E}$ mutant, and expression of the indicated proteins was determined by Western blot analysis. β-Actin served as a loading control. I, effects of INK1341 (250 nmol/L) on anchorage-independent growth of cells described in (H) were monitored using soft agar assay. Colonies in soft agar were counted after 10 days. Results are presented as a mean number of colonies relative to DMSO-treated cells (set to 100%) ± SD ($n = 3$). J, representative photographs of the colonies formed by the cells described in H.

eIF4E is frequently overexpressed in cancer (21). We examined whether overexpression of eIF4E, akin to loss of 4E-BPs, alleviates the anti-proliferative effects of the asTORi, Torin1 (9). Torin1 equally inhibited mTORC1 signaling in vector-transfected NIH3T3 cells and NIH3T3 cells that stably overexpress eIF4E (NIH3T3/4E; ref. 18), as shown by

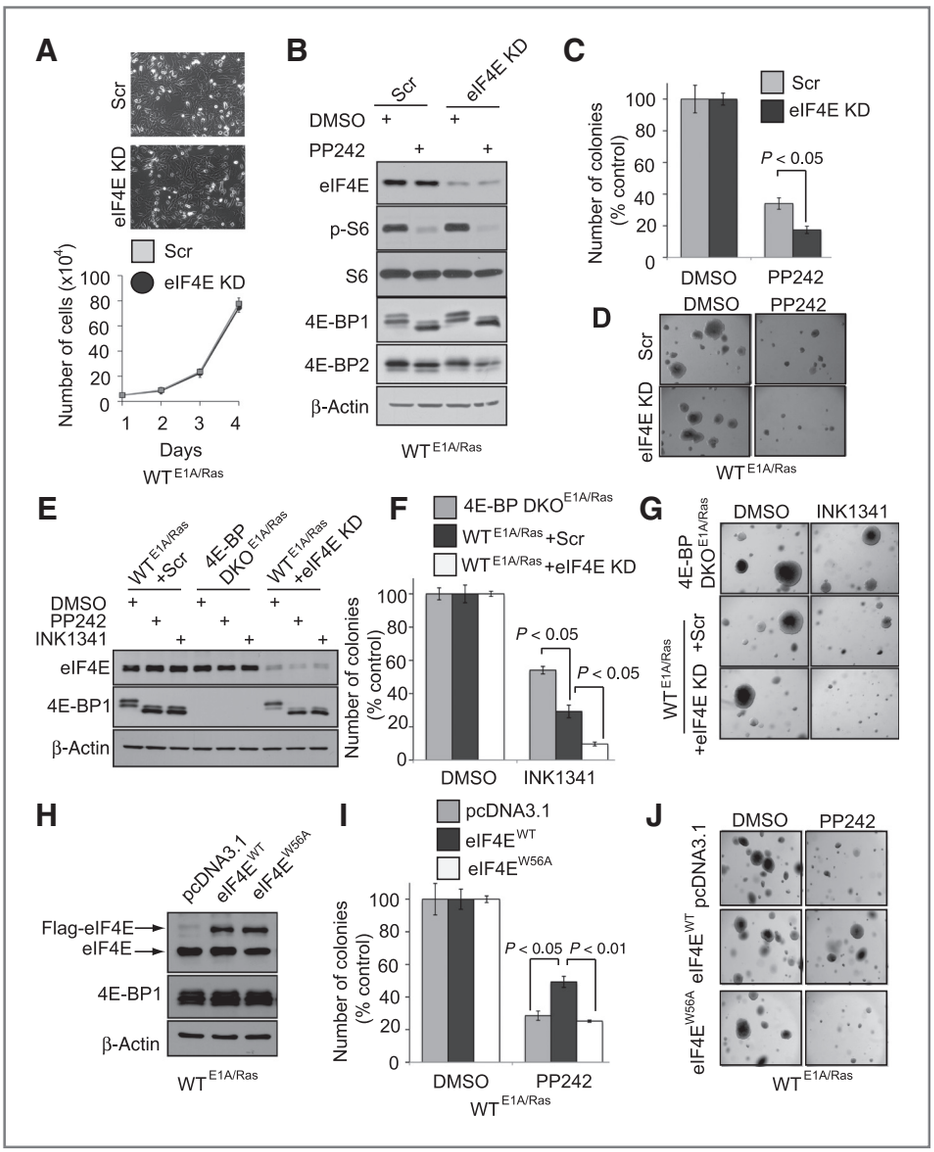

Figure 2. Elevated eIF4E/4E-BP ratio diminishes the anti-proliferative effects of asTORi. A, phase contrast images of $WT^{E1A/Ras}$ MEFs transduced with scrambled (Scr) or eIF4E shRNA (eIF4E KD; top). Proliferation rates of the indicated cells in full growth medium were determined by Trypan blue exclusion (bottom). Results are presented as mean numbers of cells ± SD ($n = 3$). B, cells described in A were treated with DMSO or PP242 (1 μmol/L) for 3 hours, and the levels and the phosphorylation status of indicated proteins were determined by Western blot analysis. β-Actin served as a loading control. C, effects of DMSO or PP242 (1 μmol/L) on anchorage-independent growth of cells described in A were monitored using a soft agar assay. Colonies in soft agar were counted after 10 days. Results are presented as a mean number of colonies relative to DMSO-treated cells (set to 100%) ± SD ($n = 3$). D, representative photographs of colonies formed by cells described in A. E, $WT^{E1A/Ras}$ MEFs transduced with scrambled ($WT^{E1A/Ras}$ + Scr) or eIF4E shRNA ($WT^{E1A/Ras}$ + eIF4E KD) and 4E-BP $DKO^{E1A/Ras}$ MEFs were treated with PP242 (1 μmol/L) or INK1341 (250 nmol/L) for 3 hours. Levels of the indicated proteins were determined by Western blot analysis. β-Actin served as a loading control. F, effects of DMSO and INK1341 (250 nmol/L) on anchorage-independent growth of cells described in E were monitored using a soft agar assay. Colonies were counted after 10 days of treatment. Results represent the mean colony number relative to a DMSO control (set to 100%) ± SD ($n = 3$). G, representative photographs of colonies formed by cells described in E. H, $WT^{E1A/Ras}$ MEFs were transfected with an empty vector (pcDNA3.1) or vector expressing Flag-tagged wild type ($eIF4E^{WT}$) or a cap-binding mutant of eIF4E ($eIF4E^{W56A}$). Levels of the indicated proteins were determined by Western blot analysis. β-Actin served as a loading control. Arrows indicate exogenous Flag-tagged (Flag-eIF4E) and endogenous eIF4E. I, effect of DMSO or PP242 (1 μmol/L) on anchorage-independent growth of cells described in H was monitored using soft agar assay. Colonies were counted after 10 days of treatment. Results represent the mean cell number relative to a DMSO control (set to 100%) ± SD ($n = 3$). J, representative photographs of colonies formed by cells described in H.

comparable reduction in the phosphorylation of 4E-BP1 and S6 (Supplementary Fig. S3A). In contrast, Torin1 inhibited proliferation and G_1 to S-phase cell-cycle progression in NIH3T3/4E cells to a dramatically lesser extent (~15%) as compared with control cells (~85%; Supplementary Fig. S3B and S3C).

To further establish that the alterations in eIF4E availability determine the anti-neoplastic effects of asTORi, we depleted eIF4E in WT$^{E1A/Ras}$ MEFs and compared the anti-neoplastic effects of PP242 with those observed in control cells. As significant eIF4E downregulation inhibits proliferation and survival (36), we selected cells in which eIF4E depletion (~50% of control) does not affect cell proliferation under optimal nutrient conditions wherein mTOR is active (Fig. 2A and B). Nonetheless, an approximate 50% decrease in eIF4E levels strongly augmented the sensitivity of WT$^{E1A/Ras}$ MEFs to PP242 (~85% reduction in colony and foci formation), as compared with control (~65%; Figs. 2C and D; Supplementary Fig. S3D–S3F). Similar results were obtained using INK1341 (Figs. 2E–G; Supplementary Fig. S3G and S3H). Suppression of neoplastic growth by asTORi was caused by the inhibition of cell-cycle progression from G_1 to S-phase, whereas asTORi did not exert a major effect on cell survival (Supplementary Fig. S4A–S4C). Importantly, the asTORi-induced inhibition of G_1–S progression was alleviated in cells with high eIF4E/4E-BP ratio (Supplementary Fig. S4A). These results support a model whereby asTORi suppress neoplastic growth by limiting eIF4E availability and cell-cycle progression.

Persistent translation of eIF4E-sensitive mRNAs renders cells refractory to asTORi

The eIF4E/4E-BP ratio dictates cap-dependent mRNA translation rates (15). Thus, we investigated whether translational activity of eIF4E is required for attenuation of the anti-neoplastic effects of asTORi, by overexpressing wild-type (eIF4E^{WT}) and a translationally inactive W56A eIF4E mutant (eIF4E^{W56A}; refs. 37, 38) in WT$^{E1A/Ras}$ MEFs. Both proteins were expressed to a comparable level (Fig. 2H). Cells overexpressing

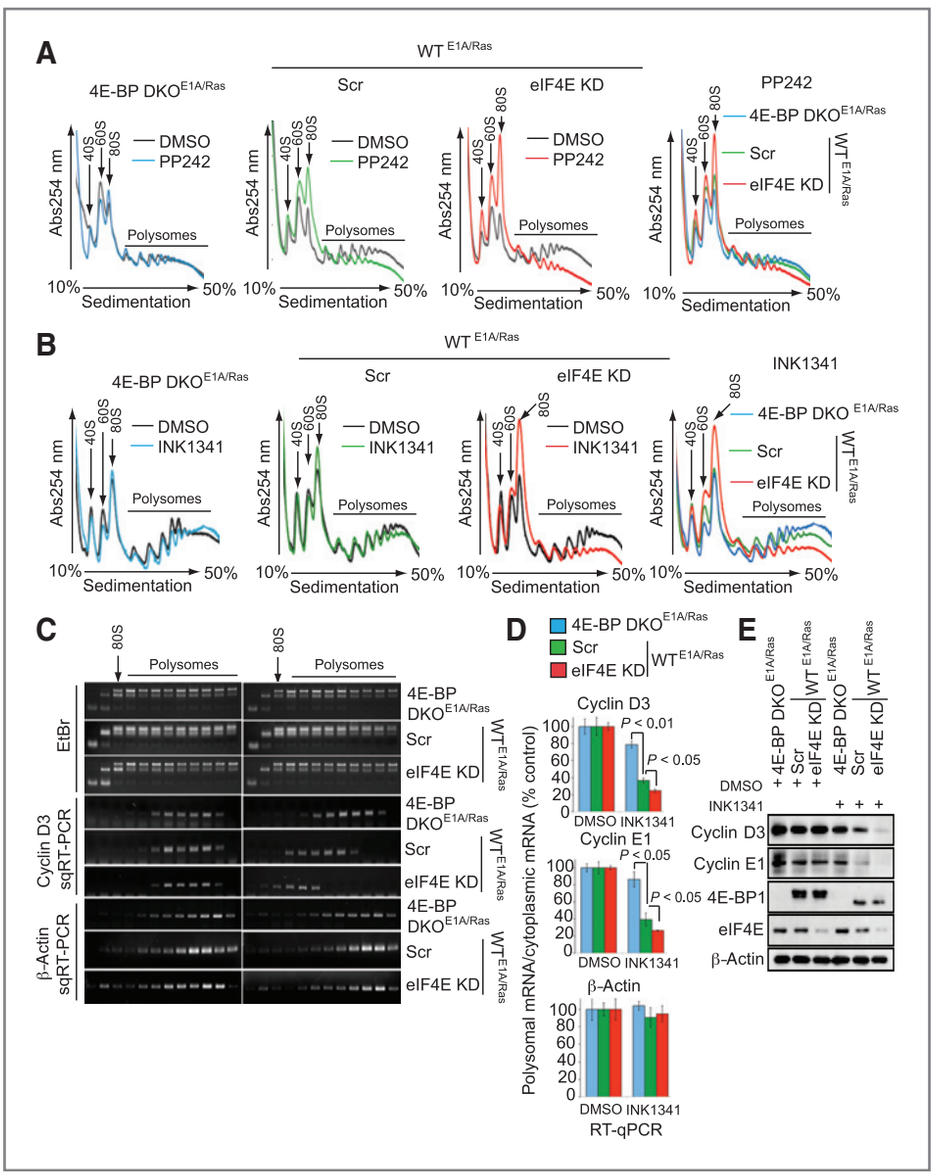

Figure 3. Increased eIF4E/4E-BP stoichiometry antagonizes the inhibitory effects of asTORi on mRNA translation. A and B, UV absorption profiles (254 nm) of ribosomes isolated from 4E-BP DKO$^{E1A/Ras}$ MEFs or WT$^{E1A/Ras}$ MEFs that were transduced with a scrambled (Scr) or eIF4E shRNA (eIF4E KD) and treated with DMSO, PP242 (1 μmol/L; A), or INK1341 (250 nmol/L; B) for 8 hours. 40S, 60S, and 80S denote the corresponding ribosomal subunits and monosome, respectively. C, RNA isolated from the fractions of DMSO- or PP242-treated cells was visualized by ethidium bromide (EtBr; top). Polysome distribution of β-actin and cyclin D3 mRNAs was determined by semiquantitative RT-PCR (sqRT-PCR; bottom). D, indicated cells were treated as described in B, and levels of the indicated mRNAs from the cytoplasmic and heavy polysome fractions (4 ribosomes and more; polysomal mRNA) were determined by qRT-PCR. Results are presented as a mean percentage of the polysomal/cytoplasmic mRNA ratio relative to DMSO control (set to 100%) ± SD ($n = 3$). E, levels of the indicated proteins in cells described in (B) were monitored by Western blot analysis. β-Actin served as a loading control.

eIF4E^{WT} exhibited significantly lower sensitivity (~50% inhibition of proliferation) to the anti-neoplastic and anti-proliferative effects of PP242 than control cells (~70%), whereas suppression of proliferation and neoplastic growth by PP242 in cells overexpressing eIF4E^{W56A} was similar to that observed in control cells (Figs. 2I and J; Supplementary Fig. S4D and S4E). Similar results were obtained in HeLa cells (Supplementary Fig. S4F–S4H).

Next, we examined the effect of PP242 and INK1341 on global mRNA translation in WT$^{E1A/Ras}$ and 4E-BP DKO$^{E1A/Ras}$ MEFs, as well as in WT$^{E1A/Ras}$ MEFs depleted of eIF4E, by studying polysome formation. The fraction of ribosomes engaged in polysomes is directly proportional to the translation initiation rate (39). Consistent with previous reports that PP242 suppresses initiation of cap-dependent mRNA translation (8), a decrease in the number of ribosomes engaged in polysomes, and a concomitant increase in 80S monosome peak was detected in all cells treated with PP242 as compared with control (Fig. 3A). However, inhibition of polysome formation by PP242 was most pronounced in WT$^{E1A/Ras}$ MEFs in which eIF4E was depleted, intermediate in control WT$^{E1A/Ras}$ MEFs, and weakest in 4E-BP DKO$^{E1A/Ras}$ MEFs (Fig. 3A). Similar results were obtained using INK1341 (Fig. 3B).

While our data show that an elevated eIF4E/4E-BP ratio mitigates the inhibition of global mRNA translation by PP242 or INK1341, the lack of a complete dissociation of polysomes indicates that the majority of mRNAs remain translationally active in asTORi-treated cells. This suggests that the resistance to asTORi is caused by the resistance of eIF4E-sensitive mRNAs to inhibition in cancer cells with elevated eIF4E/4E-BP ratio (21, 40). Thus, we investigated the effects of PP242 and INK1341 on translation of the prototypical eIF4E-sensitive mRNAs cyclin D3, and cyclin E1, as well as ß-actin mRNA, which is only marginally sensitive to changes in eIF4E (7, 22). In vehicle-treated cells, in which the sequestration of eIF4E by 4E-BPs is minimal due to the hyperphosphorylation of 4E-BPs, loss of 4E-BPs or approximately 50% depletion of eIF4E had no major impact on translation of eIF4E-senstive mRNAs (Figs. 3C–E). PP242 and INK1341 abolished the phosphorylation of 4E-BPs (Figs. 1E, 2B, and 3E) and strongly suppressed translation of the eIF4E-sensitive mRNAs cyclin D3 and E1, as well as the expression of corresponding proteins in control

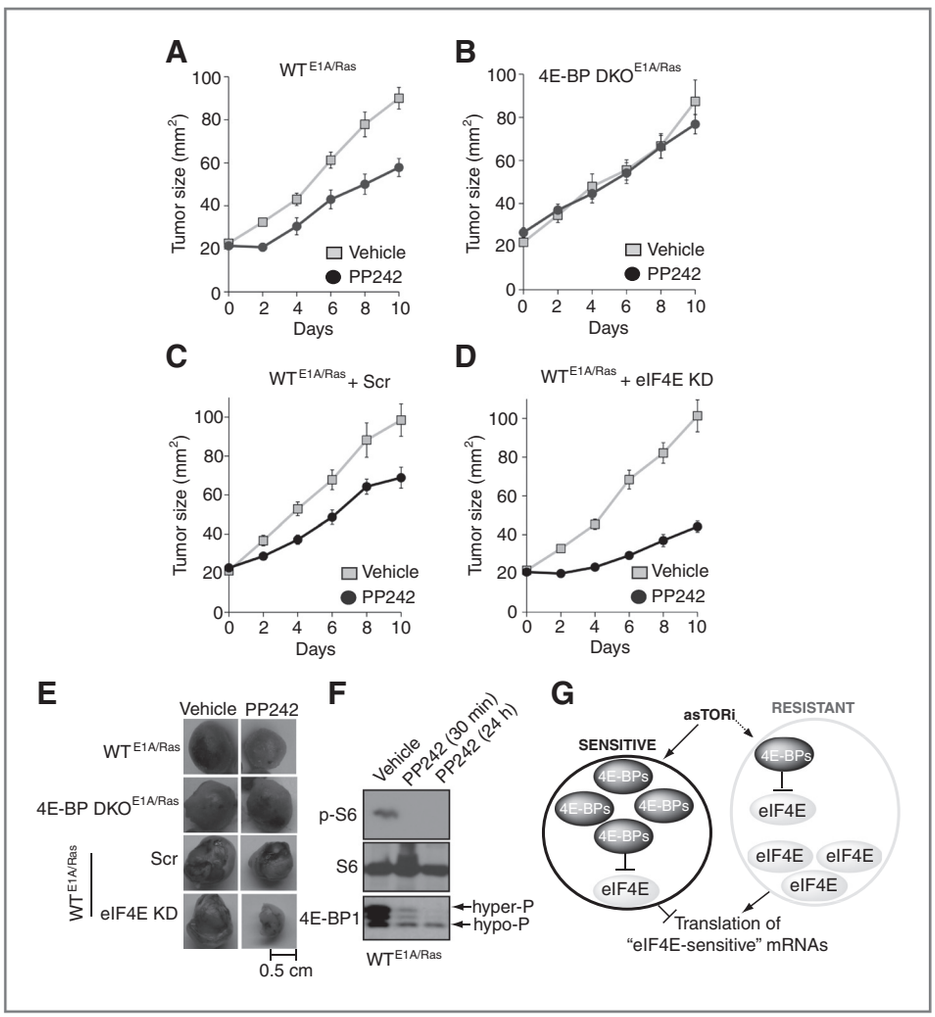

Figure 4. The eIF4E/4E-BP ratio determines the anti-neoplastic effects of PP242 *in vivo*. A and B, nude^{NCR} mice were subcutaneously implanted with 5×10^6 WT$^{E1A/Ras}$ and 4E-BP1/2 DKO$^{E1A/Ras}$ MEFs. When tumors reached palpable size (~20 mm^2), mice were injected intraperitoneally with vehicle or PP242 (60 mg/kg) daily for 10 days. Tumor growth was followed every second day, and 2-dimensional measurements were taken using a caliper. C and D, nude^{NCR} mice were subcutaneously implanted with 5×10^6 WT$^{E1A/Ras}$ MEFs infected with scrambled (Scr) or eIF4E shRNA (eIF4E KD) and treated as in A and B. E, photographs of representative tumors isolated from each group of mice. F, levels and the phosphorylation status of S6 and 4E-BP1 proteins at indicated time points in tumors described in A were determined by Western blot analysis. S6 served as loading control. Arrows indicate the hyperphosphorylated (hyper-P) and hypophosphorylated (hypo-P) forms of 4E-BP1. G, proposed model of cancer cell sensitivity to asTORi. asTORi induce sufficient sequestration of eIF4E to inhibit translation of eIF4E-sensitive mRNAs and neoplastic growth of cancer cells with low (left circle) but not high (right circle) eIF4E/4E-BP ratio.

$WT^{E1A/Ras}$ MEFs, which was further potentiated by the depletion of eIF4E (Figs. 3C–E). In stark contrast, translation of cyclin D3 and E1 mRNAs and expression of cyclin D3 and E1 proteins in 4E-BP $DKO^{E1A/Ras}$ MEFs were largely insensitive to PP242 and INK1341 (Figs. 3C–E). As expected, the translation of β-actin mRNA or expression of β-actin protein were not influenced by asTORi treatment in any of the cell lines (Figs. 3C–E). Finally, Torin1 strongly reduced cyclin D3 expression in control NIH3T3 cells, but not in NIH3T3 cells overexpressing eIF4E (Supplementary Fig. S3A). Collectively, these results show that the resistance to the anti-neoplastic effects of asTORi of cancer cells with high eIF4E/4E-BP ratio stems from the failure of asTORi to efficiently inhibit translation of eIF4E-sensitive mRNAs.

eIF4E/4E-BP ratio determines sensitivity to asTORi *in vivo*

Next, we studied the impact of perturbations in the eIF4E/4E-BP ratio on the anti-neoplastic activity of asTORi *in vivo*. Mice bearing subcutaneous tumors formed by $WT^{E1A/Ras}$ or 4E-BP $DKO^{E1A/Ras}$ MEFs were treated daily with PP242 or a vehicle. Remarkably, whereas PP242 inhibited the growth of tumors formed by $WT^{E1A/Ras}$ MEFs, tumors lacking 4E-BPs were completely resistant to PP242. Moreover, depletion of eIF4E in $WT^{E1A/Ras}$ tumors further increased their sensitivity to PP242 (Figs. 4A–E). PP242 strongly inhibited mTOR signaling *in vivo*, as illustrated by inhibition of S6 phosphorylation 30 minutes and 24 hours postinjection from tumor tissues (Fig. 4F). Thus, consistent with the *in vitro* findings, the anti-neoplastic activity of asTORi *in vivo* is predominantly established by the eIF4E/4E-BP ratio in the tumor.

Discussion

mTOR signaling is frequently dysregulated in cancer and is being targeted in clinical trials using asTORi (1, 41). However, there are currently no reliable markers that can predict the therapeutic efficacy of asTORi. Recently, several models have been proposed to explain resistance to asTORi as well as dual PI3K/mTOR kinase inhibitors in tumors. These include activation of alternative signaling pathways, such as the extracellular signal–regulated kinase pathway that can render 4E-BP1 persistently inactive despite treatment with mTOR inhibitors (42), or pathways that activate cap-independent translation of survival-promoting mRNAs (43). We have unraveled a different mechanism to explain the acquired resistance to mTOR inhibitors, whereby cancer cells become insensitive to asTORi by downregulating expression of 4E-BP1 and 2. This leads to an increase in the eIF4E/4E-BP ratio, thereby attenuating the anti-neoplastic effects of asTORi as it limits their inhibitory effect on the translation of eIF4E-sensitive mRNAs. Our model explains recent findings showing that resistance to BEZ235, a dual PI3K/mTOR inhibitor, can be acquired through amplification of the eIF4E gene (44). Thus, our results support a model whereby an elevated eIF4E/4E-BP ratio renders tumors resistant not only to asTORi (Fig. 4G) but also to dual PI3K/mTOR inhibitors.

Recent studies have proposed that the combination of mitogen-activated protein kinase with mTOR inhibitors could overcome resistance to mTOR inhibitors (42, 45). However, data presented here raise the possibility that using therapies that target eIF4E in the tumor (21, 36) may be more beneficial in cases where elevated eIF4E/4E-BP ratio is present. Moreover, our findings strongly suggest that the eIF4E/4E-BP ratio could serve as a predictive marker to tailor personalized treatments using asTORi in the clinic.

Disclosure of Potential Conflicts of Interest

No potential conflicts of interest were disclosed.

Authors' Contributions

Conception and design: T. Alain, M. Morita, A. Yanagiya, P. Metrakos, I. Topisirovic, N. Sonenberg
Development of methodology: T. Alain, M. Morita, P. Metrakos, V. Gandin, I. Topisirovic
Acquisition of data (provided animals, acquired and managed patients, provided facilities, etc.): T. Alain, M. Morita, B.D. Fonseca, A. Yanagiya, N. Siddiqui, M. Bhat, D. Zammit, V. Marcus, L.-A. Voyer, V. Gandin, Y. Liu
Analysis and interpretation of data (e.g., statistical analysis, biostatistics, computational analysis): T. Alain, M. Morita, A. Yanagiya, M. Bhat, D. Zammit, V. Marcus, P. Metrakos, Y. Liu, I. Topisirovic
Writing, review, and/or revision of the manuscript: T. Alain, M. Morita, N. Siddiqui, M. Bhat, D. Zammit, P. Metrakos, Y. Liu, I. Topisirovic, N. Sonenberg
Administrative, technical, or material support (i.e., reporting or organizing data, constructing databases): T. Alain, M. Morita, A. Yanagiya, Y. Liu
Study supervision: P. Metrakos, I. Topisirovic, N. Sonenberg

Acknowledgments

The authors thank Thomas Kucharski and Jose Teodoro for the help with flow cytometry experiments and Colin Lister, Annie Sylvestre, and Isabelle Harvey for technical assistance. T. Alain is a recipient of a fellowship from the Brain Tumour Foundation of Canada. M. Morita is a recipient of a Uehara Memorial foundation postdoctoral fellowship and a CIHR-funded Chemical Biology Postdoctoral fellowship.

Grant Support

This research was funded by grants from the CIHR and CCSRI to I. Topisirovic and N. Sonenberg and a grant from the CRS to N. Sonenberg. I. Topisirovic holds a CIHR New Investigator award.

The costs of publication of this article were defrayed in part by the payment of page charges. This article must therefore be hereby marked *advertisement* in accordance with 18 U.S.C. Section 1734 solely to indicate this fact.

Received June 20, 2012; revised September 24, 2012; accepted October 16, 2012; published OnlineFirst October 24, 2012.

References

1. Zoncu R, Efeyan A, Sabatini DM. mTOR: from growth signal integration to cancer, diabetes and ageing. Nat Rev Mol Cell Biol 2011;12:21–35.
2. Oh WJ, Jacinto E. mTOR complex 2 signaling and functions. Cell Cycle 2011;10:2305–16.
3. Menon S, Manning BD. Common corruption of the mTOR signaling network in human tumors. Oncogene 2008;27 Suppl 2:S43–51.
4. Guertin DA, Sabatini DM. The pharmacology of mTOR inhibition. Sci Signaling 2009;2:pe24.
5. Yao JC, Shah MH, Ito T, Bohas CL, Wolin EM, Van Cutsem E, et al. Everolimus for advanced pancreatic neuroendocrine tumors. N Engl J Med 2011;364:514–23.
6. Um SH, Frigerio F, Watanabe M, Picard F, Joaquin M, Sticker M, et al. Absence of S6K1 protects against age- and diet-induced

obesity while enhancing insulin sensitivity. Nature 2004;431:200–5.
7. Dowling RJ, Topisirovic I, Alain T, Bidinosti M, Fonseca BD, Petroulakis E, et al. mTORC1-mediated cell proliferation, but not cell growth, controlled by the 4E-BPs. Science 2010;328:1172–6.
8. Feldman ME, Apsel B, Uotila A, Loewith R, Knight ZA, Ruggero D, et al. Active-site inhibitors of mTOR target rapamycin-resistant outputs of mTORC1 and mTORC2. PLoS Biol 2009;7:e38.
9. Thoreen CC, Kang SA, Chang JW, Liu Q, Zhang J, Gao Y, et al. An ATP-competitive mammalian target of rapamycin inhibitor reveals rapamycin-resistant functions of mTORC1. J Biol Chem 2009;284:8023–32.
10. Garcia-Martinez JM, Moran J, Clarke RG, Gray A, Cosulich SC, Chresta CM, et al. Ku-0063794 is a specific inhibitor of the mammalian target of rapamycin (mTOR). Biochem J 2009;421:29–42.
11. Hsieh AC, Liu Y, Edlind MP, Ingolia NT, Janes MR, Sher A, et al. The translational landscape of mTOR signalling steers cancer initiation and metastasis. Nature 2012;485:55–61.
12. Benjamin D, Colombi M, Moroni C, Hall MN. Rapamycin passes the torch: a new generation of mTOR inhibitors. Nat Rev Drug Discov 2011;10:868–80.
13. Jackson RJ, Hellen CU, Pestova TV. The mechanism of eukaryotic translation initiation and principles of its regulation. Nat Rev Mol Cell Biol 2010;11:113–27.
14. Sonenberg N, Hinnebusch AG. Regulation of translation initiation in eukaryotes: mechanisms and biological targets. Cell 2009;136:731–45.
15. Pause A, Belsham GJ, Gingras AC, Donze O, Lin TA, Lawrence JC Jr, et al. Insulin-dependent stimulation of protein synthesis by phosphorylation of a regulator of 5′-cap function. Nature 1994;371:762–7.
16. Brunn GJ, Hudson CC, Sekulic A, Williams JM, Hosoi H, Houghton PJ, et al. Phosphorylation of the translational repressor PHAS-I by the mammalian target of rapamycin. Science 1997;277:99–101.
17. Gingras AC, Kennedy SG, O'Leary MA, Sonenberg N, Hay N. 4E-BP1, a repressor of mRNA translation, is phosphorylated and inactivated by the Akt(PKB) signaling pathway. Genes Dev 1998;12:502–13.
18. Lazaris-Karatzas A, Montine KS, Sonenberg N. Malignant transformation by a eukaryotic initiation factor subunit that binds to mRNA 5′ cap. Nature 1990;345:544–7.
19. Avdulov S, Li S, Michalek V, Burrichter D, Peterson M, Perlman DM, et al. Activation of translation complex eIF4F is essential for the genesis and maintenance of the malignant phenotype in human mammary epithelial cells. Cancer Cell 2004;5:553–63.
20. Ruggero D, Montanaro L, Ma L, Xu W, Londei P, Cordon-Cardo C, et al. The translation factor eIF-4E promotes tumor formation and cooperates with c-Myc in lymphomagenesis. Nat Med 2004;10:484–6.
21. Graff JR, Konicek BW, Carter JH, Marcusson EG. Targeting the eukaryotic translation initiation factor 4E for cancer therapy. Cancer Res 2008;68:631–4.
22. Mamane Y, Petroulakis E, Martineau Y, Sato TA, Larsson O, Rajasekhar VK, et al. Epigenetic activation of a subset of mRNAs by eIF4E explains its effects on cell proliferation. PLoS ONE 2007;2:e242.
23. Sorrells DL, Meschonat C, Black D, Li BD. Pattern of amplification and overexpression of the eukaryotic initiation factor 4E gene in solid tumor. J Surg Res 1999;85:37–42.
24. Jones RM, Branda J, Johnston KA, Polymenis M, Gadd M, Rustgi A, et al. An essential E box in the promoter of the gene encoding the mRNA cap-binding protein (eukaryotic initiation factor 4E) is a target for activation by c-myc. Mol Cell Biol 1996;16:4754–64.
25. Topisirovic I, Siddiqui N, Orolicki S, Skrabanek LA, Tremblay M, Hoang T, et al. Stability of eukaryotic translation initiation factor 4E mRNA is regulated by HuR, and this activity is dysregulated in cancer. Mol Cell Biol 2009;29:1152–62.
26. Rojo F, Najera L, Lirola J, Jimenez J, Guzman M, Sabadell MD, et al. 4E-binding protein 1, a cell signaling hallmark in breast cancer that correlates with pathologic grade and prognosis. Clin Cancer Res 2007;13:81–9.
27. Yamaguchi S, Ishihara H, Yamada T, Tamura A, Usui M, Tominaga R, et al. ATF4-mediated induction of 4E-BP1 contributes to pancreatic beta cell survival under endoplasmic reticulum stress. Cell Metab 2008;7:269–76.
28. Yanagiya A, Suyama E, Adachi H, Svitkin YV, Aza-Blanc P, Imataka H, et al. Translational homeostasis via the mRNA cap-binding protein, eIF4E. Mol Cell 2012;46:847–58.
29. Rousseau D, Gingras AC, Pause A, Sonenberg N. The eIF4E-binding proteins 1 and 2 are negative regulators of cell growth. Oncogene 1996;13:2415–20.
30. Gingras AC, Gygi SP, Raught B, Polakiewicz RD, Abraham RT, Hoekstra MF, et al. Regulation of 4E-BP1 phosphorylation: a novel two-step mechanism. Genes Dev 1999;13:1422–37.
31. Rong L, Livingstone M, Sukarieh R, Petroulakis E, Gingras AC, Crosby K, et al. Control of eIF4E cellular localization by eIF4E-binding proteins, 4E-BPs. RNA 2008;14:1318–27.
32. Poulin F, Gingras AC, Olsen H, Chevalier S, Sonenberg N. 4E-BP3, a new member of the eukaryotic initiation factor 4E-binding protein family. J Biol Chem 1998;273:14002–7.
33. Alain T, Lun X, Martineau Y, Sean P, Pulendran B, Petroulakis E, et al. Vesicular stomatitis virus oncolysis is potentiated by impairing mTORC1-dependent type I IFN production. Proc Natl Acad Sci U S A 2010;107:1576–81.
34. Dowling RJ, Zakikhani M, Fantus IG, Pollak M, Sonenberg N. Metformin inhibits mammalian target of rapamycin-dependent translation initiation in breast cancer cells. Cancer Res 2007;67:10804–12.
35. Mader S, Lee H, Pause A, Sonenberg N. The translation initiation factor eIF-4E binds to a common motif shared by the translation factor eIF-4 gamma and the translational repressors 4E-binding proteins. Mol Cell Biol 1995;15:4990–7.
36. Graff JR, Konicek BW, Vincent TM, Lynch RL, Monteith D, Weir SN, et al. Therapeutic suppression of translation initiation factor eIF4E expression reduces tumor growth without toxicity. J Clin Invest 2007;117:2638–48.
37. Marcotrigiano J, Gingras AC, Sonenberg N, Burley SK. Cocrystal structure of the messenger RNA 5′ cap-binding protein (eIF4E) bound to 7-methyl-GDP. Cell 1997;89:951–61.
38. Matsuo H, Li H, McGuire AM, Fletcher CM, Gingras AC, Sonenberg N, et al. Structure of translation factor eIF4E bound to m7GDP and interaction with 4E-binding protein. Nat Struct Biol 1997;4:717–24.
39. Warner JR, Knopf PM, Rich A. A multiple ribosomal structure in protein synthesis. Proc Natl Acad Sci U S A 1963;49:122–9.
40. Silvera D, Formenti SC, Schneider RJ. Translational control in cancer. Nat Rev Cancer 2010;10:254–66.
41. Zask A, Verheijen JC, Richard DJ. Recent advances in the discovery of small-molecule ATP competitive mTOR inhibitors: a patent review. Expert Opin Ther Patents 2011;21:1109–27.
42. She QB, Halilovic E, Ye Q, Zhen W, Shirasawa S, Sasazuki T, et al. 4E-BP1 is a key effector of the oncogenic activation of the AKT and ERK signaling pathways that integrates their function in tumors. Cancer Cell 2010;18:39–51.
43. Muranen T, Selfors LM, Worster DT, Iwanicki MP, Song L, Morales FC, et al. Inhibition of PI3K/mTOR leads to adaptive resistance in matrix-attached cancer cells. Cancer Cell 2012;21:227–39.
44. Ilic N, Utermark T, Widlund HR, Roberts TM. PI3K-targeted therapy can be evaded by gene amplification along the MYC-eukaryotic translation initiation factor 4E (eIF4E) axis. Proc Natl Acad Sci U S A 2011;108:E699–708.
45. Mendoza MC, Er EE, Blenis J. The Ras-ERK and PI3K-mTOR pathways: cross-talk and compensation. Trends Biochem Sci 2011;36:320–8.